ELSEVIER

Journal of Magnetism and Magnetic Materials 195 (1999) 708–732

Journal of magnetism and magnetic materials

www.elsevier.com/locate/jmmm

The particle interaction effects in the field-cooled and zero-field-cooled magnetization processes

C. Papusoi Jr.*

ISTG, MESA Research Institute, University of Twente, P.O. Box 217, 7500 AE Enschede, Netherlands

Received 16 September 1998; received in revised form 21 January 1999

Abstract

The present theories explaining the mechanism of particle interaction within a fine particle system driven by the thermal agitation assign the increase of the interaction strength either to an increase of the particle anisotropy due to the environment reaction to its dipole moment, or to the occurrence of a collective state. The particle interaction effects on the field-cooled (FC) and zero-field-cooled (ZFC) magnetization curves are the *anisotropy effect*, referring to the increase of the temperature T_{MAX}, corresponding to the ZFC curve maximum, with increasing sample volume concentration, and the *mean-field effect*, referring to the flattening of both, FC and ZFC, magnetization curves with increasing sample demagnetizing factor, without altering T_{MAX} in the low applied field limit. We demonstrate that the Onsager mean-field model is able to recover an increase of the particle anisotropy with increasing sample volume concentration using a cavity having the shape of an oblate ellipsoid, the eccentricity increasing with increasing sample volume concentration. The proposed explanation is the formation of particle clusters having a uniaxial symmetry in the particle arrangement (chain-of-particles). We show that the anisotropy effect of interactions is due to not only an increase of the particle anisotropy with increasing sample volume concentration, but also to a temperature-dependent interaction field distribution due to the local non-homogeneity of the particle dispersion. The proposed model is able to recover the experimental FC and ZFC initial susceptibility curves for various concentrations of γ-Fe_2O_3 nanoparticle systems.

PACS: 75.60

Keywords: FC process; ZFC process; Field-linear sample response domain; Two-level model; Master equation; Superparamagnetism; Reaction anisotropy; Interaction field distribution

1. Introduction

The present theories describing the mechanism of particle interaction within a fine particle system driven by the thermal agitation, are actually at their initial stages. According to some authors [1–7], an increase of the interaction strength with increasing sample volume concentration $C_V = n\bar{V}$ (n is the mean number of

* Permanent address: Faculty of Physics, "Al.I. Cuza" University, 11 Bd. Copou, 6600 Iasi, Romania, Fax: + 40-32-213-330.
E-mail address: cpapusoi@uaic.ro (C. Papusoi)

0304-8853/99/$ - see front matter
PII: S0304-8853(99)00288-7

particles per sample unit volume and $\bar{V}$ is the mean particle volume) enhances the particle anisotropy as a consequence of the particle environment reaction to its dipole magnetic moment. Other approaches [8–14], generally based on the Landau theory of phase transitions, show that for high-volume concentrations, the interactions give rise to a collective behavior of the particle moments, like that encountered in spin–glass systems. The purpose of this paper is to offer a more unitary picture about the particle interaction role in the FC and ZFC magnetization processes in the frame of a mean-field model.

The field-cooled (FC) magnetization is acquired during a cooling process, in the presence of a magnetic field $\boldsymbol{H}_{\text{appl}}$, from a temperature T_{HIGH}, high enough to ensure a superparamagnetic behavior, down to a temperature T_{LOW}, low enough to minimize the thermal relaxation effects. The zero-field-cooled (ZFC) magnetization is acquired during the heating of the sample from T_{LOW} to T_{HIGH} in the presence of a magnetic field $\boldsymbol{H}_{\text{appl}}$, the sample being previously demagnetized by cooling from T_{HIGH} to T_{LOW} in the absence of the applied field.

The FC and ZFC magnetization curves evidence two important effects of the particle interactions:

- *the anisotropy effect*, regarding the increase of the temperature T_{MAX}, corresponding to the ZFC curve maximum, with increasing sample volume concentration C_V;
- *the mean-field effect*, referring to the dependence of both the FC and ZFC magnetization curves, on the sample shape (both are flattening with increasing sample demagnetizing factor), the T_{MAX} temperature being unaffected by the sample shape for a given C_V, in the low applied field limit.

The above-mentioned effects are present in the sample linear response domain with respect to the applied field, in agreement with the AC susceptibility measurements [2], being a direct consequence of the particle interactions.

The samples we have used for evidencing the interaction effects on the FC and ZFC curves contain γ-Fe_2O_3 nanoparticles, prepared by the chemical precipitation method described in Refs. [15,16], embedded in a solid, polymer matrix (Table 1). For each particle size, we dispose of samples having different volume concentrations, denoted by (C/50), (C/25), (C/5) and (C/1) as C_V increases. Particles were previously studied by TEM in Ref. [15], and were found to be almost spherical, having a length-to-width ratio of about 1.2 : 1.3. The samples have the shape of discs, 5 mm in diameter and 0.5 mm in thickness. The magnetic moment measurements were performed using a commercial SQUID-RF magnetometer.

Table 1

Samples	Volume concentrations C_V ($\times 10^{-3}$)	Intrinsic anisotropy constant $K_{\text{tot}} = K_V + K_S 6/D$		Mean particle diameter $\bar{D}$ (nm)	Particle diameter distribution			
		$K_V \times 10^5$ (erg/cm^3)	$K_S \times 10^{-2}$ (erg/cm^2)		Gaussian		Lognormal	
					$\bar{D}$ (nm)	σ	D_{median} (nm)	σ
26A(C/50)	4.95	0.9	1.1	9.8	9.8	0.35		
26A(C/1)	203	0.9	1.1	9.8	9.8	0.35		
4D(C/50)	7.38	1.15	0.7	7	7	0.4		
4D(C/25)	12.1	1.15	0.7	7	7	0.4		
4D(C/5)	47	1.15	0.7	7	7	0.4		
4D(C/1)	202	1.15	0.7	7	7	0.4		
36A(C/50)	8.11	1	3.2	4.9			4.7	0.27
36A(C/1)	196	1	3.2	4.9			4.7	0.27
51A(C/50)	9.42	1	6.5	2.9			2.8	0.27
51A(C/1)	202	1	6.5	2.9			2.8	0.27

Table 2

Sample	26A		4D				36A		51A	
	C/50	C/1	C/50	C/25	C/5	C/1	C/50	C/1	C/50	C/1
$\langle D\rangle/\bar{D}$	4.7	1.4	4.1	3.5	2.2	1.4	4.0	1.4	3.8	1.4
H_{dip} (Oe)	1.9	70.6	2.8	4.5	18.2	70.6	3	70.6	3.5	70.6

The particle intrinsic anisotropies $K_{\mathrm{tot}} = K_V + K_S 6/D$, where D is the particle diameter, K_V is the magnetostatic anisotropy constant (greater than the magnetocrystalline anisotropy for our particles) and K_S the surface anisotropy constant [17], were studied in Ref. [18] for the low interacting samples (C/50), the results being presented in Table 1.

The temperature variation law for the particle spontaneous magnetization, deduced on the basis of high-field measurements [3] is $M_S(T) = M_S(0)(1 - aT^{2.2})$ for the samples 26A and 4D, where $a = 4.4 \times 10^{-7}$ for 26A(C/50), $a = 4.7 \times 10^{-7}$ for 26A(C/1), $a = 4.4 \times 10^{-7}$ for 4D(C/50) and 4D(C/25), $a = 4.7 \times 10^{-7}$ for 4D(C/5), $a = 4.9 \times 10^{-7}$ for 4D(C/1), and, respectively, $M_S(T) = M_S(0)(1–2.5 \times 10^{-6} T^2)$ for both the 36A and 51A samples, where $M_S(0) \cong 370$ emu/cm^3 [18].

The fact that both the anisotropy and mean-field effects are present in the sample field-linear response domain allows us to use a linear mean-field theory [19]. This choice has the following advantages:

- a rigorous expression for the superparamagnetic magnetization, deduced on the basis of the Boltzmann equilibrium distribution, could be used;
- the two-level model for the thermal relaxation, valid in the high-energy barrier limit, could be used;
- the Maxwell equations could be used in the calculus of the interaction field.

Nevertheless, there are some restrictions concerning the validity of the linear theory. The local non-homogeneity of the particle dispersion could give rise to interaction fields strong enough to yield a field non-linear particle magnetization. For having a picture about the dipole interactions strength for different samples and volume concentrations, we present in Table 2 the mean interparticle spacing $\langle D\rangle$ [15] and the corresponding dipole field created by a particle at the distance $\langle D\rangle$ from its centre (by assuming that the particle spontaneous magnetization $M_S = 370$ emu/cm^3) for the 10 samples mentioned above. For the samples having low-volume concentrations, like (C/50) and (C/25), the dipole interaction fields are approximately $H_{\mathrm{dip}} \approx 1–5$ Oe, which is the order of magnitude of the applied fields yielding a field-linear magnetization for all the samples we use, as it will be shown later. This is not the case for the most concentrated samples (C/5) and (C/1), where the dipole fields $H_{\mathrm{dip}} \approx 18–70$ Oe become high enough to induce a field non-linear particle magnetization.

Consequently, it is possible that, at least for the concentrations (C/5) and (C/1), the samples exhibit a linear behavior with respect to the applied field (for H_{appl} enough low), but a non-linear one with respect to the intrinsic dipole interactions.

2. Theory

2.1. The mean interaction field

The fact that both effects of interactions on the FC and ZFC curves are present in the field-linear sample response domain strongly suggests that the Debye mean-field model, where the interaction field is

proportional to the sample magnetization, does not adequately describe the interaction effects in the presence of the thermal relaxation. The observation that, in the low applied field limit, the sample demagnetizing factor does not influence the T_{MAX} temperature but C_V does, shows that an interaction field proportional to the sample magnetization would never account for the anisotropy effect, because the mean-field parameter plays the same role as the demagnetizing factor. This statement is demonstrated in Ref. [19], and, more generally, in Ref. [20] for any value of the applied field in the case of a particle system having the easy axis parallel to the applied field direction. Onsager [21] pointed out that the Debye model offers an expression averaged over the equilibrium states of the particle system and not an instantaneous expression for the interaction field, disregarding the reaction of the medium to the particle field. Dormann [1] has calculated a reaction field in the frame of a discrete pair-of-particle model, but he used some restricting hypothesis, like

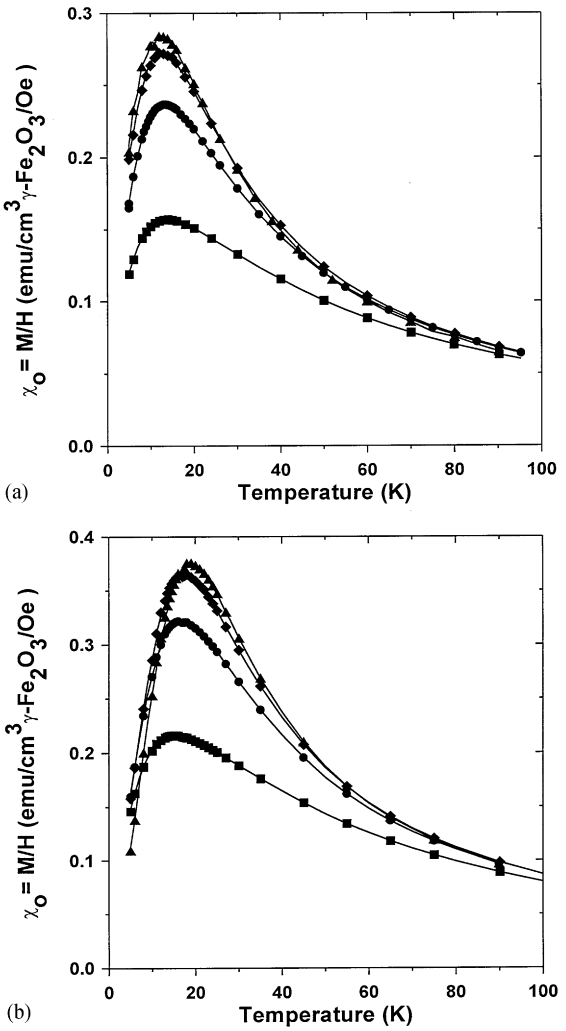

Fig. 1. (a) The $\chi_0 = M/H_{appl}$ susceptibility for the sample 51A(C/50): $H_{appl} = 5$ Oe (▲), 50 Oe (◆), 100 Oe (●), 300 Oe (■) (acting parallel to the sample plane). (b) The $\chi_0 = M/H_{appl}$ susceptibility for the sample 51A(C/1): $H_{appl} = 5$ Oe (▲), 50 Oe (◆), 100 Oe (●), 300 Oe (■) (acting parallel to the sample plane).

he imposed the particle moment fluctuations to undergo in the vicinity of some privileged axis, the same for all the particles, which was not sufficiently argued. He has shown that dipole interactions just increase the particle anisotropy along the privileged axis, with decreasing interparticle spacing. This statement could easily be checked by examining the connection between the width of the sample linear response domain (with respect to the applied field) and the sample volume concentration. If the particle interactions are only increasing the particle anisotropy, one should always notice a broadening of the field-linear response domain with increasing C_V, due to the increase of the particle anisotropy field.

The field-linear behavior of the sample magnetization could be studied using the susceptibility $\chi_0 = M/H_{\text{appl}}$ (M is the sample magnetization) which coincides with the initial susceptibility $\chi_i = \mathrm{d}M/\mathrm{d}H_{\text{appl}}|_{H_{\text{appl}}=0}$ (being independent of the applied field) in the low-applied field domain. For this reason, we have plotted the curves M/H_{appl} corresponding to the ZFC process, for different values of H_{appl} and we have tracked the lower limit of the applied field for which the M/H_{appl} curves begin to differ. We have noticed (Figs. 1 and 2) that for the most diluted samples (C/50) the linear response domain broadens from about 10 Oe for 26A(C/50) to about 50 Oe for the 51A(C/50) sample, which is obviously a consequence of increasing particle surface anisotropy with decreasing particle size [18]. One also notices that an increase of C_V always narrows the linear response domain, an effect which is more evident when the particle size is larger, i.e. the surface anisotropy is lower. This observation is supported by the fact that the temperature corresponding to the ZFC curve maximum T_{MAX} decreases with increasing applied field and this decrease is more rapid when the sample volume concentration increases. In Ref. [18] it is shown that the shift of T_{MAX} towards higher values is a consequence of the field non-linear behavior of the superparamagnetic magnetization while the decrease of T_{MAX} is the consequence of decreasing barriers separating the free energy minima. Thus, the applied field decreases the energy barriers faster in the interacting case than in the low interacting case, revealing that increasing interaction strength is not equivalent just to an increase of the particle intrinsic anisotropy, which would yield an opposite effect.

According to the sample fabrication method [15], the particle easy axis are almost randomly oriented, ensuring a global isotropic character to the magnetic properties of our samples. The particles are homogeneously dispersed in a solid polymer matrix, the volume concentration being C_V. For sufficiently low applied fields and a homogeneous particle dispersion, the sample is equivalent to a continuous, homogeneous and isotropic medium, of initial permeability $\mu(T)$, which is connected to the particle system's initial susceptibility $\langle\chi\rangle$ through $\mu(T) = 1 + 4\pi C_V\langle\chi\rangle$. The low values of the particle eccentricity $e = 0.55$–0.64, found by TEM in Ref. [15], enables us to assume a spherical particle shape. The particle intrinsic anisotropy (including both the magnetostatic and surface anisotropies) is supposed to be uniaxial, given the dominance of the surface anisotropy with respect to the magnetocrystalline one, of density $K(V, T) = K_V(T) + K_S 6/D$. We shall suppose that the particle volume distribution function is $F(V)$ ($\int_0^\infty F(V)\,\mathrm{d}V = 1$) and the temperature variation law for the particle spontaneous magnetization is $M_S(T)$. In order to find the initial FC and ZFC permeabilities of the particle dispersion, we shall suppose that the medium is unbounded (given that $\mu(T)$ depends only on the magnetization mechanism, being independent of the sample shape).

In the frame of the Stoner–Wohlfarth model [22], the free energy of a particle having the volume V and easy axis orientation described by the unit vector $\hat{k}$ is

$$E = V[K(V, T)\sin^2\theta - \boldsymbol{H}_{\text{eff}}\cdot\boldsymbol{M}_S(T)], \tag{1}$$

θ being the angle between the particle easy axis and its magnetic moment, and $\boldsymbol{H}_{\text{eff}}$ is the effective field acting at the particle site.

According to the Onsager model [21], the effective interaction field could be found using the superposition principle:

$$\boldsymbol{H}_{\text{eff}} = \boldsymbol{H}_{\text{C}} + \boldsymbol{H}_{\text{R}}. \tag{2}$$

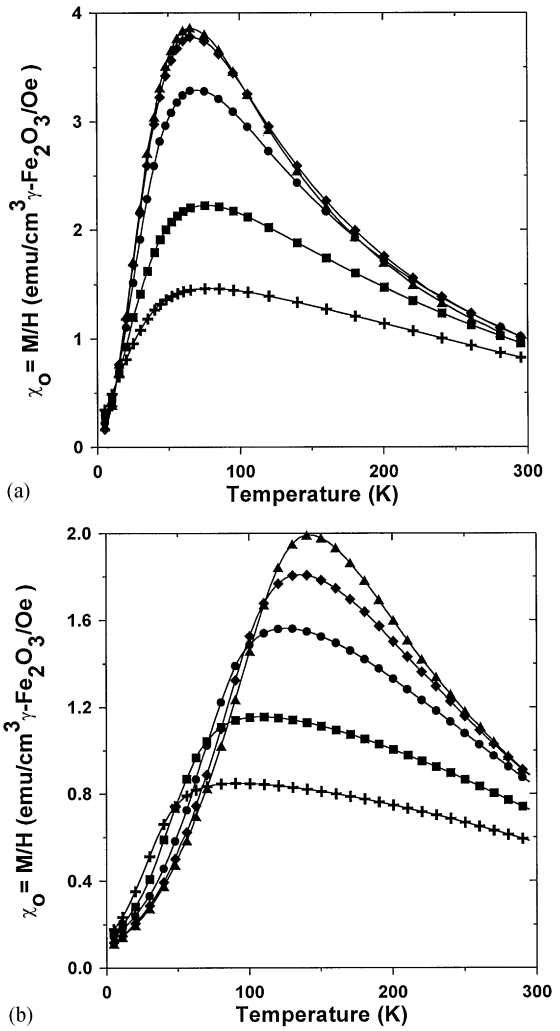

Fig. 2. (a) The $\chi_0 = M/H_{appl}$ susceptibility for the sample 26A(C/50): $H_{appl} = 5$ Oe (▲), 10 Oe (◆), 20 Oe (●), 50 Oe (■), 100 Oe (+) (acting parallel to the sample plane). (b) The $\chi_0 = M/H_{appl}$ susceptibility for the sample 26A(C/1): $H_{appl} = 5$ Oe (▲), 10 Oe (◆), 20 Oe (●), 50 Oe (■), 100 Oe (+) (acting parallel to the sample plane).

The first term in Eq. (2), known as the *cavity field*, acts at the inner of the cavity obtained by drawing out the particle from the medium, in the presence of the internal field $\boldsymbol{H}$. The second term in Eq. (2), known as the *reaction field*, comes from the medium magnetized by the particle itself, in the absence of the applied field.

The Onsager model is not able to provide a general method for finding the shape and size of the cavity, these being generally dictated by the features of the interacting system, as Onsager pointed out [21]. Under these circumstances, the Onsager theory could be improved by establishing some connections between the cavity size and the characteristic quantities of the medium like the volume concentration C_V. We shall demonstrate that an increase of the particle anisotropy as a result of increasing particle interaction strength, as suggested by Dormann [1], could be interpreted on the basis of the Onsager model using an ellipsoidal

cavity, of eccentricity dependent on the sample volume concentration. The cavity eccentricity is expected to increase with increasing C_V as a result of the broken symmetry in the particle environment permeability due the non-regular arrangement of the neighboring particles with respect to the given one.

Let us consider a dipole having a permanent magnetic moment $\boldsymbol{m} = \boldsymbol{M}_S V$ (where V is the particle volume) placed at the center of an ellipsoidal cavity, having the semiaxis $a > b > c$, performed in a continuous, homogeneous and isotropic medium of permeability $\mu(T) > 1$. In order to find the reaction field acting on the dipole, one should solve the Neumann problem:

$$\Delta V = 0 \text{ (excepting at the cavity center)}, \tag{3}$$

$$\left[\mu \frac{\partial V_{\text{ext}}}{\partial n} - \frac{\partial V_{\text{int}}}{\partial n}\right]_S = 0, \quad (V_{\text{ext}} - V_{\text{int}})|_S = 0,$$

($\boldsymbol{B} = \boldsymbol{H} + 4\pi\boldsymbol{M}$, $\nabla \cdot \boldsymbol{B} = 0$, $\nabla \times \boldsymbol{H} = 0 \Rightarrow \boldsymbol{H} = -\nabla V$, $\Delta V = 0$) where V_{ext}, V_{int} are the scalar potentials inside and outside the cavity, S is the cavity surface and $\hat{n}$ is the unit vector of the outward normal to the cavity surface. It is easy to show that the reaction field components along the cavity axis are

$$H_{R,i} = \frac{3m_i}{abc} N_i(1 - N_i) \frac{\mu - 1}{\mu - (\mu - 1)N_i}, \quad i = \{x, y, z\}, \tag{4}$$

where N_i are the demagnetizing coefficients of the ellipsoid ($\sum_{i=\{x,y,z\}} N_i = 1$). As expected, the reaction field is uniform inside an ellipsoidal cavity.

In the particular case of an oblate ellipsoid ($a = b > c$), Eq. (4) ascertains that the energy of the reaction field is of the same type as that corresponding to a uniaxial anisotropy along the short axis (c) of the ellipsoid:

$$E_{\text{R}} = -\frac{1}{2}\boldsymbol{H}_R \cdot \boldsymbol{m} = \frac{2\pi}{V_{\text{cav}}} N_X(N_X - N_Z) \frac{[\mu + (\mu - 1)N_Z](\mu - 1)}{[\mu - (\mu - 1)N_X][\mu - (\mu - 1)N_Z]} m_Z^2, \tag{5}$$

where $V_{\text{cav}} = 4\pi abc/3$ is the cavity volume. For a spherical cavity, the reaction anisotropy is zero as a consequence of the parallelism between the reaction field and the particle magnetic moment.

Strictly speaking, the existence of a reaction anisotropy is a consequence of the tensor character of the local permeability. Still, the identification of its components and their correlation to the global (macroscopic)

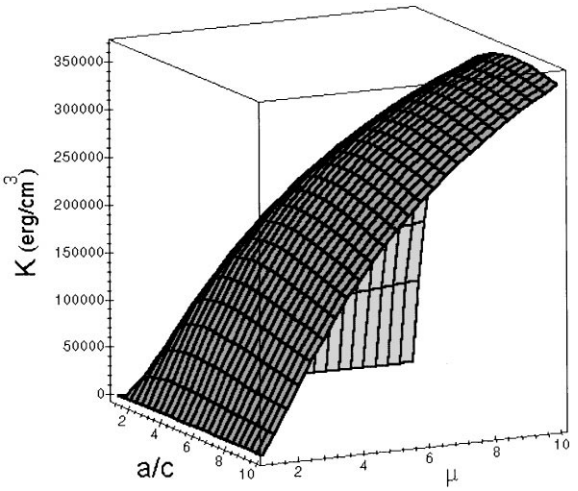

Fig. 3. The reaction anisotropy of a dipole placed at the center of a cavity having the shape of an oblate ellipsoid ($a = b > c$).

permeability of the particle dispersion is quite difficult. A more practical alternative, though approximate, is a particular choice of the Onsager cavity according to the symmetry imposed by the space configuration of the neighboring particles, the particle dispersion being further considered as homogeneous and isotropic. Thus, the Onsager cavity shape is mainly dictated by the features of the neighboring particles arrangement and not by the particle shape. The choice of an oblate ellipsoidal shape for the cavity corresponds to a particle agglomeration along the Oz axis (parallel to the short axis of the ellipsoidal cavity), like a chain of particles oriented along the Oz axis. Such configuration could ensure an anisotropy along the Oz axis. The oblate ellipsoidal shape for the cavity is not critical, the latter one corresponding to the lowest symmetry degree for the particle arrangement.

In Fig. 3 we have presented the reaction anisotropy as a function of the cavity axis ratio and medium permeability. One notices that the reaction anisotropy increases monotonically with increasing medium permeability, but it exhibits a maximum with respect to a/c. The assumption that the particle volume is equal to the cavity volume, used in the calculus of the reaction anisotropy, is reasonable given that the reaction anisotropy range for our samples is ensured by low values of the cavity eccentricity, of the same order of magnitude as those corresponding to a physical particle, as it will be shown in the following.

Let us consider the ellipsoidal cavity acted upon by a uniform internal field $\boldsymbol{H}$ (different from the applied field $\boldsymbol{H}_{\text{appl}}$ due to the sample shape). In order to find the field acting inside the cavity, one should solve the Neumann problem:

$$\Delta V = 0, \quad \left[\mu \frac{\partial V_{\text{ext}}}{\partial n} - \frac{\partial V_{\text{int}}}{\partial n}\right]_S = 0, \quad (V_{\text{ext}} - V_{\text{int}})|_S = 0. \tag{6}$$

One easily finds the following expressions for the components of the cavity field (acting inside the cavity) along the cavity axis:

$$H_{\text{C},i} = \frac{\mu}{\mu - (\mu - 1)N_i} H_i, \quad i = \{x, y, z\}. \tag{7}$$

2.2. The FC and ZFC initial susceptibilities

Using expression (2) for the mean interaction field and assuming an oblate ellipsoidal shape for the Onsager cavity, the particle free energy (1) can be written as

$$E = V[K_{\text{tot}}(V, T) \sin^2 \theta - H_{\text{C}}(T) M_S(T) \cos(\psi^* - \theta)], \tag{8}$$

where ψ^* is the angle between the field $\boldsymbol{H}_{\text{C}}$, acting inside the cavity, and the short axis Oz of the cavity. We have used the following notations:

$$K_{\text{tot}}(V, T) = K(V, T) + 2\pi N_X (N_Z - N_X) \frac{[\mu + (\mu - 1)N_Z](\mu - 1)}{[\mu - (\mu - 1)N_X][\mu - (\mu - 1)N_Z]} M_S^2(T), \tag{9}$$

$$H_{\text{C}} \cos \psi^* = H d_1 \cos \psi, \tag{10}$$

$$H_{\text{C}} \sin \psi^* = H d_2 \sin \psi, \tag{11}$$

$$d_1 = \frac{\mu}{\mu - (\mu - 1)N_Z}, \tag{12}$$

$$d_2 = \frac{\mu}{\mu - (\mu - 1)N_X}, \tag{13}$$

where ψ is the angle between the internal field $\boldsymbol{H}$ and the short axis of the cavity. For simplicity, we have assumed that the particle intrinsic anisotropy is collinear with the short axis of the cavity (i.e. with the reaction anisotropy axis). We shall use the additional notations:

$$K_{\text{tot}}(V, T) = K_0 K'_{\text{tot}}(V, T), \tag{14}$$

$$M_S(T) = M_0 M'_S(T), \tag{15}$$

where K_0 and M_0 are constants satisfying the condition $H_{K_0} = 2K_0/M_0 \gg H$.

The evolution of the (V, ψ) system towards the equilibrium state could be described by the master equation [19,23,24]:

$$\frac{\mathrm{d}P_1}{\mathrm{d}t} = -W_{12}P_1 + W_{21}P_2, \tag{16}$$

where P_1 and P_2 are the occupation probabilities of the two energy levels ($P_1 + P_2 = 1$), W_{21} is the transition rate to the energy minimum orientation closer to the internal field direction, while W_{12} corresponds to the thermally activated transitions to the other minimum. The transition rates for a (V, ψ) particle system are approximately given by the Arrhenius–Néel law:

$$W_{ij} = f_0 \exp(-\beta g_i), \quad i \neq j = \overline{1, 2}, \tag{17}$$

where $\beta = K_{\text{tot}}V/(k_{\text{B}}T)$, $g_i = \Delta E_{ij}/K_{\text{tot}}V$, ΔE_{12}, ΔE_{21} are the energy barriers separating the two minima of Eq. (8), and

$$f_0 \cong \frac{2}{\sqrt{\pi}} \frac{\gamma_0 K_{\text{tot}}}{M_S(0)} \frac{\sqrt{\beta}}{\eta_r + 1/\eta_r}. \tag{18}$$

$\gamma_0 \approx 2 \times 10^7\ \text{s}^{-1}$ is the electron gyromagnetic ratio, $\eta_r = \eta\gamma_0 M_S$, η being the damping constant.

The linear expression of the master Eq. (16) is

$$\frac{\mathrm{d}(\delta P_1)}{\mathrm{d}t} = -2W\delta P_1 + 2W\beta \frac{M'_S(T)}{K'_{\text{tot}}(V, T)} d_1 \cos\psi\,, \tag{19}$$

where $\delta P_1 \equiv \partial P_1/\partial h|_{h=0}$, $h = H/H_{K_0}$, $\beta = K_{\text{tot}}V/k_{\text{B}}T$, $W = f_0 \exp(-\beta)$, the initial condition being $\delta P_1|_{t=0} = 0$. The solutions of Eq. (19) are

$$\delta P_1(T) = \begin{cases} 0, & T \leqslant T_{\text{cr}}(V) \\ \beta(T) \dfrac{M'_S(T)}{K'_{\text{tot}}(V, T)} d_1(T) \cos\psi, & T > T_{\text{cr}}(V) \end{cases} \tag{20}$$

for the ZFC process, and for the FC process;

$$\delta P_1(T) = \begin{cases} \beta(T_{\text{cr}}) \dfrac{M'_S(T_{\text{cr}})}{K'_{\text{tot}}(V, T_{\text{cr}})} d_1(T_{\text{cr}}) \cos\psi, & T \leqslant T_{\text{cr}}(V) \\ \beta(T) \dfrac{M'_S(T_{\text{cr}})}{K'_{\text{tot}}(V, T)} d_1(T) \cos\psi, & T > T_{\text{cr}}(V). \end{cases} \tag{21}$$

For a constant temperature rate, the critical temperature $T_{\text{cr}}(V)$ for both the FC and ZFC processes is the solution of the blocking condition [19]

$$\mathrm{d}\tau/\mathrm{d}T|_{T=T_{\text{cr}}} = -|\mathrm{d}T/\mathrm{d}t|^{-1}, \tag{22}$$

where τ is the (V, ψ) system relaxation time for constant temperature and applied field, given by $1/\tau = W_{12} + W_{21}$.

The reduced initial susceptibility (with respect to the internal field H) of the identical particle system (V, ψ), $\delta\rho \equiv \partial\rho/\partial h|_{h=0}$, where $\rho = M/M_S(T)$, M being the magnetization of the (V, ψ) system, is

$$\delta\rho = \frac{M'_S(T)}{K'_{\text{tot}}(T)}\, d_2(T) \sin^2\psi + 2\cos\psi\delta P_1. \tag{23}$$

The superparamagnetic initial susceptibility for a (V, ψ) system given by the two-level model is inefficient given that at high temperatures, the particle moment orientations are widely dispersed around the free energy minima. For this reason, we shall replace the expression for the initial susceptibility given by the two-level model by the coefficient of h from the h power series expansion of the Boltzmann expression for the superparamagnetic reduced magnetization [25]. One obtains

$$\delta\rho(T) = \begin{cases} \dfrac{M'_S}{K'_{\text{tot}}}\, d_2 \sin^2\psi, & T \leqslant T_{\text{cr}}(V), \\ \dfrac{M_S V K_0}{M_0 k_B T}\left[d_2 \sin^2\psi + (2d_1\cos^2\psi - d_2\sin^2\psi)\dfrac{I_2}{I_0}\right], & T > T_{\text{cr}}(V) \end{cases} \tag{24}$$

for the ZFC process, and respectively:

$$\delta\rho(T) = \begin{cases} \dfrac{M'_S}{K'_{\text{tot}}}\, d_2 \sin^2\psi + 2\beta(T_{\text{cr}})\dfrac{M'_S(T_{\text{cr}})}{K'_{\text{tot}}(T_{\text{cr}})}\, d_1(T_{\text{cr}})\cos^2\psi & T \leqslant T_{\text{cr}}(V), \\ \dfrac{M_S V K_0}{M_0 k_B T}\left[d_2 \sin^2\psi + (2d_1\cos^2\psi - d_2\sin^2\psi)\dfrac{I_2}{I_0}\right], & T > T_{\text{cr}}(V) \end{cases} \tag{25}$$

for the FC process, where $I_n = \int_0^{\pi} \exp(-\beta\sin^2\theta)\cos^n\theta\sin\theta\,\mathrm{d}\theta$.

In the frame of the continuous medium hypothesis, the permeability of the given particle surroundings does not depend either on its volume or on its easy axis orientation. Thus, by taking into account the particle volume distribution and the random easy-axis distribution, one obtains the following expression for the initial susceptibility of the particle dispersion $\delta M = \mathrm{d}M/\mathrm{d}H|_{H=0}$:

$$\frac{\mu - 1}{4\pi} = C_V\langle\chi\rangle = C_V \frac{M_S(T)M_0}{2K_0}\frac{1}{\bar{V}}\int_0^{\pi/2}\mathrm{d}\psi\int_0^{\infty}\delta\rho\sin\psi V F(V)\,\mathrm{d}V. \tag{26}$$

Using Eqs. (24)–(26), one obtains the following integral-differential equations for the particle dispersion initial permeability:

$$\frac{\mu - 1}{4\pi} = \frac{1}{3}M_S^2\frac{C_V}{\bar{V}}\left\{\frac{1}{k_B T}\int_0^{V_{\text{cr}}} \upsilon V^2 F(V)\,\mathrm{d}V + \int_{V_{\text{cr}}}^{\infty}\frac{d_2}{K_{\text{tot}}} V F(V)\,\mathrm{d}V\right\} \tag{27}$$

for the ZFC process, and for the FC process

$$-\frac{1}{M_S^2}\dot{M}_S(\mu - 1) + \frac{1}{M_S}\dot{\mu} = \frac{4\pi}{3}\frac{C_V}{\bar{V}}\left\{\frac{\dot{M}_S T - M_S}{k_B T^2}\int_0^{V_{\text{cr}}}\upsilon V^2 F(V)\,\mathrm{d}V + \frac{M_S}{k_B T}\int_0^{V_{\text{cr}}}\dot{\upsilon}V^2 F(V)\,dV + \int_{V_{\text{cr}}}^{\infty}\left(d_2\frac{\dot{M}_S K_{\text{tot}} - M_S\dot{K}_{\text{tot}}}{K_{\text{tot}}^2} + \frac{M_S}{K_{\text{tot}}}\dot{d}_2\right)V F(V)\,\mathrm{d}V\right\} \tag{28}$$

where $\upsilon = d_2 + (d_1 - d_2)I_2/I_0$. We have used the following notations: $\dot{\mu} = \mathrm{d}\mu/\mathrm{d}T$, $\dot{M}_S = \mathrm{d}M_S/\mathrm{d}T$, $\dot{\upsilon} = \mathrm{d}\upsilon/\mathrm{d}T$, $\dot{K}_{\mathrm{tot}} = \mathrm{d}K_{\mathrm{tot}}/\mathrm{d}T$. The initial condition for Eq. (27), at the temperature T_{LOW}, is the solution of the transcendent equation

$$\frac{\mu - 1}{4\pi} = \frac{1}{3} M_S^2 \frac{C_V}{\bar{V}} \int_0^\infty \frac{d_2}{K_{\mathrm{tot}}} V F(V)\, \mathrm{d}V. \tag{29}$$

The initial condition for Eq. (28), at the temperature T_{HIGH}, is the solution of the transcendent equation

$$\frac{\mu - 1}{4\pi} = \frac{1}{3} M_S^2 \frac{1}{k_{\mathrm{B}} T} \frac{C_V}{\bar{V}} \int_0^\infty \upsilon V^2 F(V)\, \mathrm{d}V. \tag{30}$$

Experimentally, one measures the magnetic moment of a sample having a certain shape, acted upon by a uniform applied magnetic field $\boldsymbol{H}_{\mathrm{appl}}$. The value and orientation of the internal field $\boldsymbol{H}$ with respect to the applied field $\boldsymbol{H}_{\mathrm{appl}}$ depend on the sample shape. If the latter is ellipsoidal, the components of the magnetization (per unit volume of ferromagnetic content) along the ellipsoid axis are

$$M_i = \frac{1}{4\pi C_V} \frac{\mu - 1}{1 + (\mu - 1)N_i} H_{\mathrm{appl},i}\,, \tag{31}$$

where N_i ($i = 1, 3$) are the demagnetizing coefficients of the ellipsoid ($\sum_{i=1}^{3} N_i = 1$). $H_{\mathrm{appl},i}$ are the components of the applied field along the ellipsoid axis. Eq. (31) shows that the sample shape does not influence the temperature T_{MAX}.

The integral-differential Eqs. (27) and (28) were numerically solved using the DASSL solver from the SLATEC library. In the simulations performed for evidencing the linear effects of interactions, we have used the following parameter values: $K_V = 10^5$ erg/cm^3, $M_S = 370$ emu/cm^3, $H_{\mathrm{appl}} = 5$ Oe, $N = 0$, a Gaussian particle diameter distribution ($\bar{D} = 7 \times 10^{-7}$ cm, $\sigma = 0.4$) and a random orientation of the cavity short axis with respect to the internal field. The temperature rate was assumed to be constant $|\mathrm{d}T/\mathrm{d}t| = 10^{-2}$ K/s and the reduced damping constant from Eq. (18) was considered as $\eta_r = 1$, according to Ref. [2].

From Fig. 4a and Fig. 4b, one remarks that the cavity axis ratio plays a negligible role for $C_V \approx 10^{-3}$ and becomes important for $C_V \approx 10^{-1}$. As one can notice in Fig. 4, for low values of the sample volume concentration ($C_V \approx 10^{-3}$), the medium initial permeability approaches the value corresponding to vacuum $\mu(T) \approx 1$, while for $C_V \approx 10^{-1}$ the permeability may reach high values $\mu(T) \approx 10$. This increases the reaction anisotropy (Fig. 5a and Fig. 5b) which is different in the FC and ZFC processes, having a similar temperature dependence as the permeability in the two processes.

2.3. The non-linear interactions

For low values of the interparticle spacing, the resultant field created by the neighboring particles at a given particle site, in the absence of the applied field, may be sufficiently high to give rise to a field non-linear particle magnetization. The most simple way for taking into account the non-linear interactions is to assign them to the existence of a temperature-dependent interaction field distribution. Let us suppose that at a given particle site an effective field $\boldsymbol{H}_{\mathrm{eff}}$ acts which includes two contributions:

$$\boldsymbol{H}_{\mathrm{eff}} = \boldsymbol{H}_{\mathrm{m}} + \boldsymbol{H}_{\mathrm{i}}. \tag{32}$$

The field denoted by $\boldsymbol{H}_{\mathrm{m}}$ (calculated, for example, using the Onsager model), is a mean-field characterizing the particle long-range interactions. This field correlates the particle interactions with the particle system's initial susceptibility, which is a global, macroscopic quantity.

The local interaction field $\boldsymbol{H}_{\mathrm{i}}$ characterizes the short-range particle interactions. It is expected that the particle dispersion non-homogeneity gives rise to an interaction field distribution of zero mean $\langle \boldsymbol{H}_{\mathrm{i}} \rangle = 0$

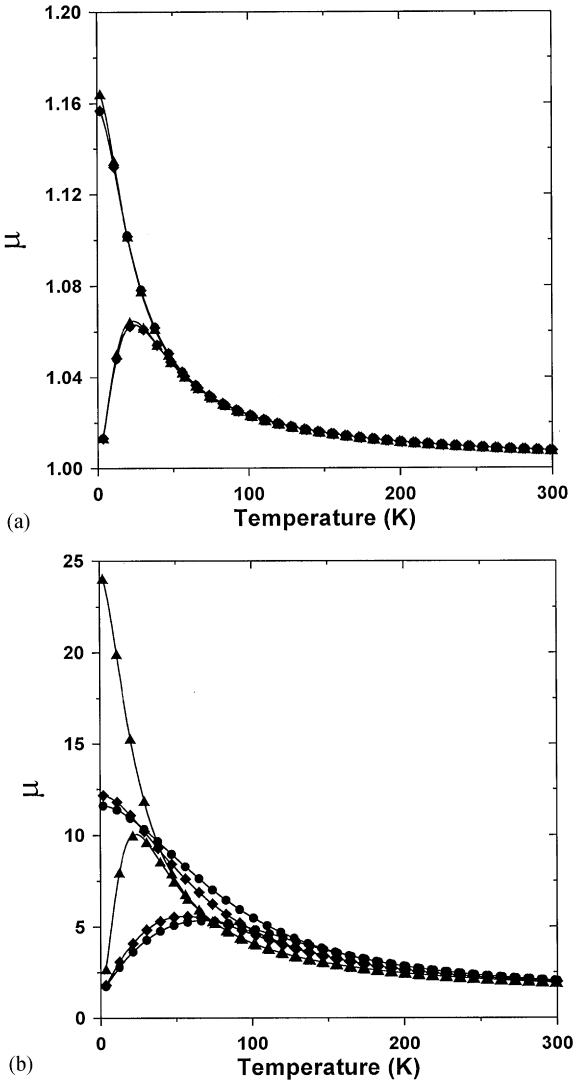

Fig. 4. The FC and ZFC initial permeabilities for $C_V = 10^{-3}$ (a) and respectively $C_V = 10^{-2}$ (b) for $a/c = 1$ (▲), 2 (◆), 3 (●).

which superposes on the mean interaction field. Such a distribution is obviously temperature dependent, being negligible at high temperatures because an increase of the temperature minimizes the effects of the particle collective behavior [6–8].

A distribution of interaction fields may influence the magnetization of a particle system only by the field non-linear effects which it could create. Thus, the interaction field distribution is expected to influence the particle critical temperature spectrum, directly by acting on the energy barriers and indirectly by influencing the particle anisotropy induced by the reaction field (which depends on the global permeability). At the same time, the interaction field distribution influences directly the medium permeability by modifying the particle free energy minima.

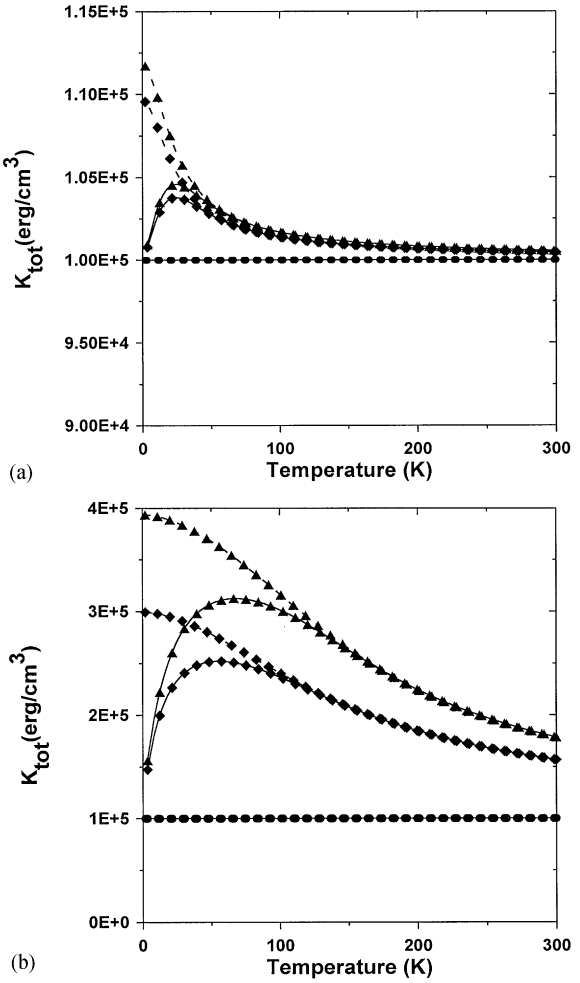

Fig. 5. The total particle anisotropy (intrinsic + reaction) in the FC (dashed line) and ZFC (solid line) processes for $C_V = 10^{-3}$ (a) and respectively $C_V = 10^{-1}$ (b) for $a/c = 1$ (▲), 2 (◆), 3 (●).

The effects of such a field distribution could be evaluated on the basis of the first two orders master equations with respect to the internal field H. The field zero-order master equation enables the study of the non-linear effect of the interaction field distribution on the occupation probabilities of the particle free energy minima, while the field first-order master equation enables the study of the linear effects created by the Onsager mean field. The two equations are obviously coupled, a fact which makes it very difficult to solve the first-order master equation due to the presence of some mixed terms (dependent on the critical temperature spectrum via the solution of the zero-order master equation). The coupling between the two master equations may be raised by making the simplifying assumption that the occupation probabilities of the free energy minima are $P_{10} = P_{20} = 1/2$. This assumption gives a slightly higher value for the blocked initial susceptibility in the two processes FC and ZFC, though offering a reasonable approximation.

For an interaction field $\boldsymbol{H}_i(T)$, one finds the following approximate expressions for the initial susceptibility of the particle system having the volume V, after averaging over the random easy axis distribution:

$$\langle \delta\rho(T)\rangle_\psi \cong \begin{cases} \frac{2}{3} H_{K_0} t_1 \dfrac{1}{1-(H_i t_1)^2}\, d_2, & T \leqslant T_{cr}(V), \\ H_{K_0} \dfrac{M_S V}{k_B T} L'\left(\dfrac{M_S V H_i}{k_B T}\right)\upsilon, & T > T_{cr}(V) \end{cases} \tag{33}$$

for the ZFC process, and for the FC process,

$$\langle \delta\rho(T)\rangle_\psi \cong \begin{cases} \frac{2}{3} H_{K_0}\left[t_1 \dfrac{1}{1-(H_i t_1)^2}\, d_2 + \beta(T_{cr}) t_1 (T_{cr}(d_1(T_{cr}))\right], & T \leqslant T_{cr}(V), \\ H_{K_0} \dfrac{M_S V}{k_B T} L'\left(\dfrac{M_S V H_i}{k_B T}\right)\upsilon, & T > T_{cr}(V) \end{cases} \tag{34}$$

$L(x) = cth(x) - 1/x$ is the Langevin function, $L'(x) = \mathrm{d}L/\mathrm{d}x$ and $t_1 = M_S/(2K_{tot})$.

Noticing that the initial susceptibilities (33) and (34) are even functions of H_i, one may approximately consider that the role of the interaction field distribution could be played by a representative field $H_i^*(T) = \sqrt{\overline{H_i(T)}}$ (for a Gaussian distribution $G(H_i)$, $H_i^*(T) = H_\sigma(T)$. We obtain the medium initial permeability for the following integral-differential equations:

$$\frac{\mu-1}{4\pi} = M_S C_V \frac{1}{\bar{V}} \left\{ \frac{M_S}{k_B T} \int_0^{V_{cr}(H_i^*)} L'\left(\frac{M_S V H_i^*}{k_B T}\right)\upsilon V^2 F(V)\,\mathrm{d}V + \frac{2}{3}\int_{V_{cr}(H_i^*)}^{\infty} \frac{t_1 d_2}{1-(H_i^* t_1)^2}\, V F(V)\,\mathrm{d}V \right\} \tag{35}$$

for the ZFC process, and for the FC process,

$$\frac{\mathrm{d}}{\mathrm{d}T}\left(\frac{\mu-1}{M_S}\right) = 4\pi C_V \frac{1}{\bar{V}} \left\{ \int_0^{V_{cr}(H_i^*)} \frac{\mathrm{d}}{\mathrm{d}T}\left[\frac{M_S}{k_B T} L'\left(\frac{M_S V H_i^*}{k_B T}\right)\upsilon\right] V^2 F(V)\,\mathrm{d}V + \frac{2}{3}\int_{V_{cr}(H_i^*)}^{\infty} \frac{\mathrm{d}}{\mathrm{d}T}\left[\frac{t_1 d_2}{1-(H_i^* t_1)^2}\right] V F(V)\,\mathrm{d}V \right\}. \tag{36}$$

The initial condition for Eq. (35), at the temperature T_{LOW}, is the solution of the transcendent equation

$$\frac{\mu-1}{4\pi} = \frac{2}{3} M_S C_V \frac{1}{\bar{V}} \int_0^{\infty} \frac{t_1 d_2}{1-(H_i^* t_1)^2}\, V F(V)\,\mathrm{d}V, \tag{37}$$

and, respectively, for Eq. (36), the initial condition at the temperature T_{HIGH} is the solution of the equation

$$\frac{\mu-1}{4\pi} = M_S^2 \frac{1}{k_B T} \frac{C_V}{\bar{V}} \int_0^{\infty} L'\left(\frac{M_S V H_i^*}{k_B T}\right)\upsilon V^2 F(V)\,\mathrm{d}V. \tag{38}$$

For evidencing the effects of the interaction field given by Eq. (32) on the FC and ZFC magnetization curves, we have numerically solved Eqs. (35) and (36) using the following parameter values: $K_V = 10^5$ erg/cm^3, $M_S = 370$ emu/cm^3, $H_{appl} = 5$ Oe, $N = 0$, $|\mathrm{d}T/\mathrm{d}t| = 10^{-2}$ K/s and $\eta_r = 1$. We have considered a Gaussian particle size distribution, of parameters $\bar{D} = 7\times10^{-7}$ cm and $\sigma = 0.4$. The function describing the temperature dependence of the interaction field H_i^* was considered $H_i^*(T) = (A/\sqrt{2\pi}\,T)\exp(-T^2/(2T^{*2}))$ where A and T^* are two fitting parameters.

From Fig. 6 one may notice that the non-linear interaction could create a similar effect to that of a reaction anisotropy, i.e. it causes a shift of the T_{MAX} temperature towards higher values with increasing interaction field strength. This effect is due to the role played by the interaction field H_i^* which, on the one hand,

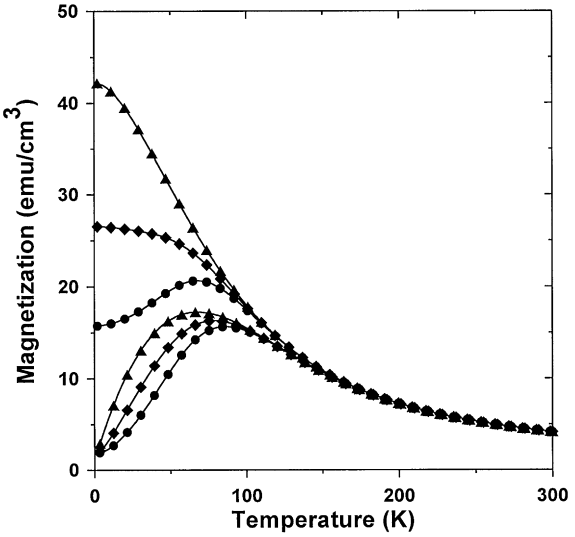

Fig. 6. The FC and ZFC magnetization curves for $C_V = 0.1$, $a/c = 3$, $T^* = 50$ K and $A = 0$ Oe (▲), 10^4 Oe (◆), 1.5×10^4 Oe (●).

decreases the superparamagnetic initial susceptibility (which approaches to saturation at low temperatures), and, on the other, it shifts the critical temperature spectrum towards lower values (by decreasing the energy barriers), thus enhancing the superparamagnetic particle fraction at low temperatures.

The interaction field H_i^* may also be responsible for a maximum of the FC curve. This effect, often encountered for spin–glass systems and highly concentrated particle systems, was previously assigned to the difference between the cooling and heating temperature rates in an FC process [3]. However, such difference should be of several orders of magnitude for interpreting this effect, unlikely to those experimentally encountered. Also, the fact that a maximum of the FC curve occurs only for samples having high-volume concentrations or some clustering degree, supports our conclusion that the maximum of the FC curve is a consequence of the non-linear effects of particle interactions. In addition, with increasing H_i^*, the ZFC curves become more concave while the FC curves more convex in the low-temperature domain, effects experimentally encountered for fine particle systems with increasing C_V [15].

3. Experiment

In the following, we present the theoretical $\chi_t(T) = (\mu - 1)/\{4\pi C_V[1 + (\mu - 1)N]\}$ and experimental $\chi_e(T) = M/H_{appl}$ curves representing the FC and ZFC initial susceptibilities for the ten samples described in the introduction. In all the figures presenting the experimental data, the initial susceptibility χ_e was divided by a scaling factor C which was found by fit. As we have pointed out in Ref. [18], this factor does not present a physical significance, being mostly due to experimental errors of measuring the sample mass and concentration and also due to the correction of the superconducting coil remanent field, which becomes of the same order of magnitude as the applied field in the range $H_{appl} = 1$–5 Oe. However, the applied field values do not affect the temperature dependence of the FC and ZFC initial susceptibilities as long as they are sufficiently low to ensure a field-linear sample magnetization. The fit of the FC and ZFC curves was performed by assuming a constant temperature rate $|dT/dt| = 0.01$ K/s for both the FC and ZFC processes. The reduced damping constant was considered as $\eta_r = 1$.

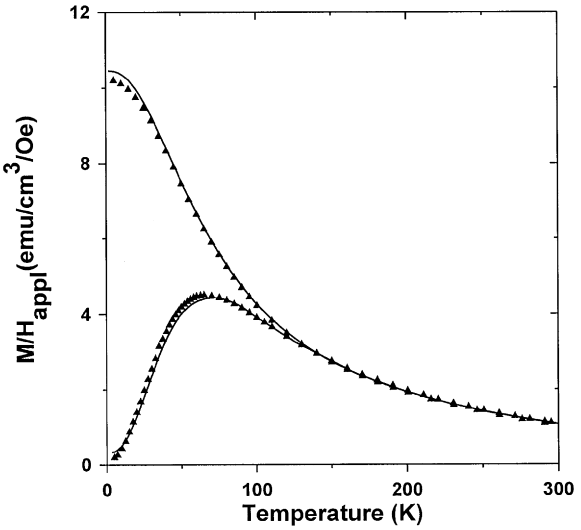

Fig. 7. The FC and ZFC initial susceptibilities for the sample 26A(C/50), measured (χ_c/C) (▲) and calculated (solid line); $H_{appl} = 5$ Oe is parallel to the sample plane.

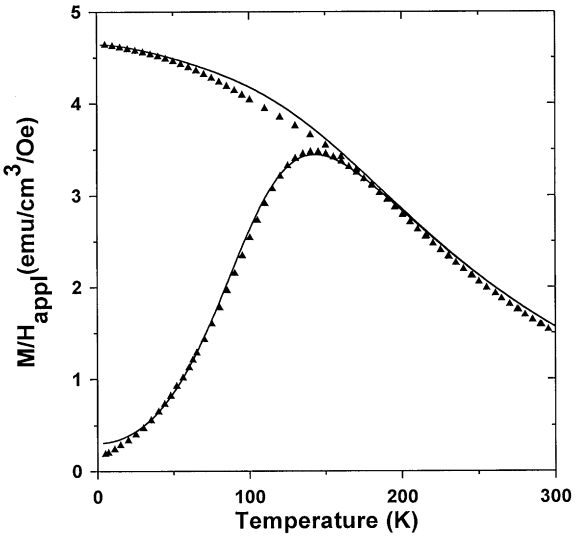

Fig. 8. The FC and ZFC initial susceptibilities for the sample 26A(C/1), measured (▲) and calculated (solid line); $H_{appl} = 5$ Oe is parallel to the sample plane.

The experimental and calculated FC and ZFC initial susceptibility curves for the samples 26A(C/50) and 26A(C/1) are presented in Figs. 7 and 8, for 4D(C/50), 4D(C/25), 4D(C/5) and 4D(C/1) in Figs. 9–12, for 36A(C/50) and 36A(C/1) in Figs. 13 and 14, and for 51A(C/50) and 51A(C/1) in Fig. 15a, Fig. 15b and Fig. 16.

The applied field values H_{appl} and the sample parameters given by the fit of the FC and ZFC curves, like those corresponding to the interaction field H_i^* (A and T^*, the sample demagnetizing factor N, the scaling factor C and the cavity axis ratio a/c, are presented in Table 3 for the ten samples studied.

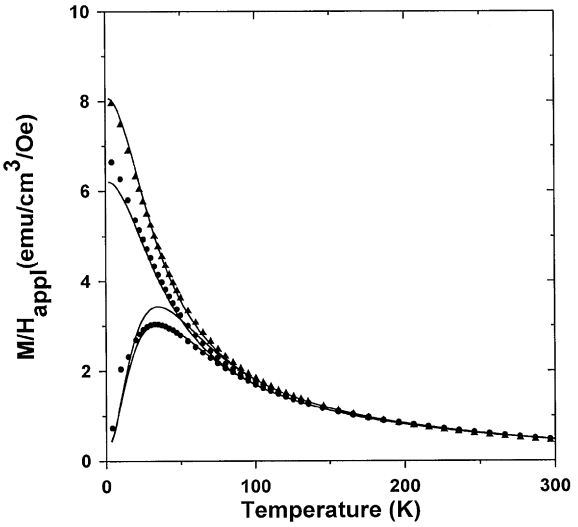

Fig. 9. The FC and ZFC initial susceptibilities for the sample 4D(C/50), measured (symbols) and calculated (solid line); $H_{\text{appl}} = 5$ Oe acts parallel (▲) respectively perpendicular (●) to the sample plane.

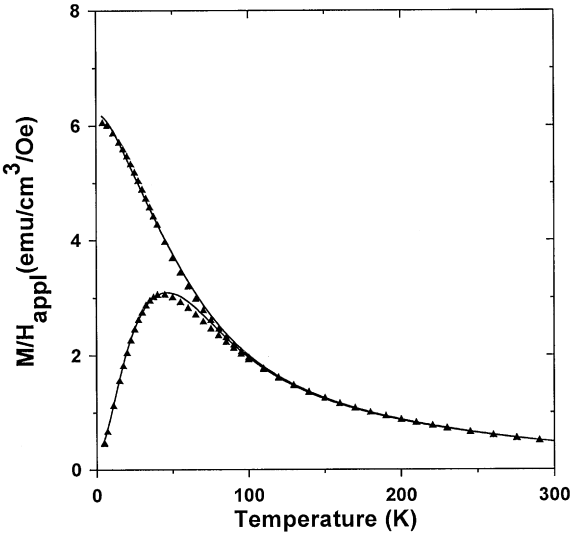

Fig. 10. The FC and ZFC initial susceptibilities for the sample 4D(C/25), measured (▲) and calculated (solid line); $H_{\text{appl}} = 5$ Oe acts parallel to the sample plane.

4. Conclusions

Both the mean-field and the anisotropy effects of interactions on the FC and ZFC magnetization curves are present in the field-linear sample response domain. In the low-applied field limit, the Debye expression for

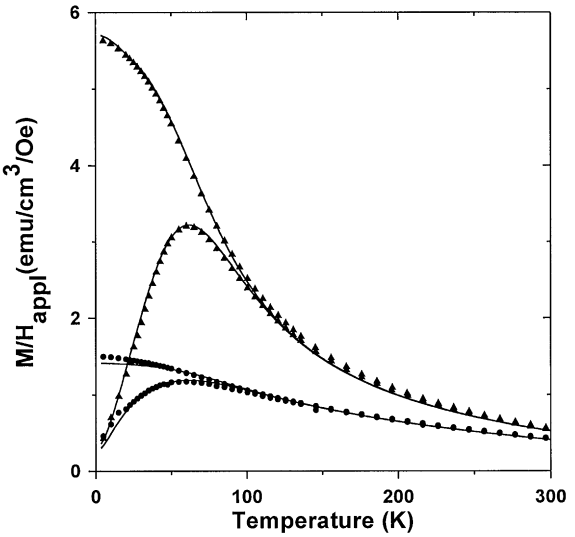

Fig. 11. The FC and ZFC initial susceptibilities for the sample 4D(C/5), measured (symbols) and calculated (solid line); $H_{\text{appl}} = 1$ Oe acts parallel (▲) respectively perpendicular (●) to the sample plane.

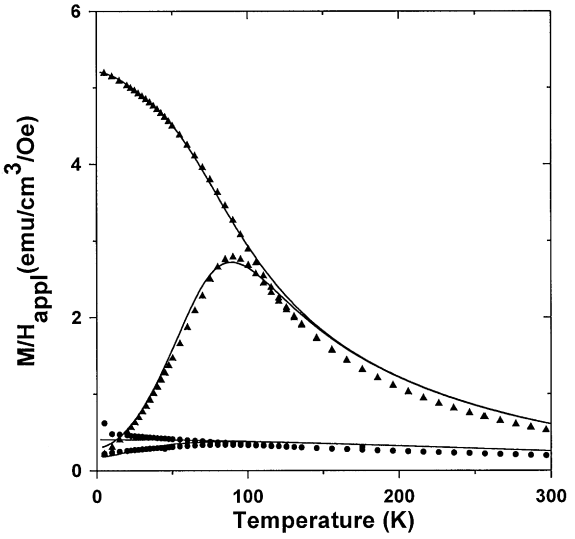

Fig. 12. The FC and ZFC initial susceptibilities for the sample 4D(C/1), measured (symbols) and calculated (solid line); $H_{\text{appl}} = 1$ Oe acts parallel (▲) respectively perpendicular (●) to the sample plane.

the interaction field is able to account only for the mean-field effect of interactions, because the critical temperature spectrum is not affected by the mean-field parameter. According to Onsager, this result is due to the fact that the Debye model offers an averaged (over the equilibrium states of the particle system) expression for the interaction field, and not an instantaneous one.

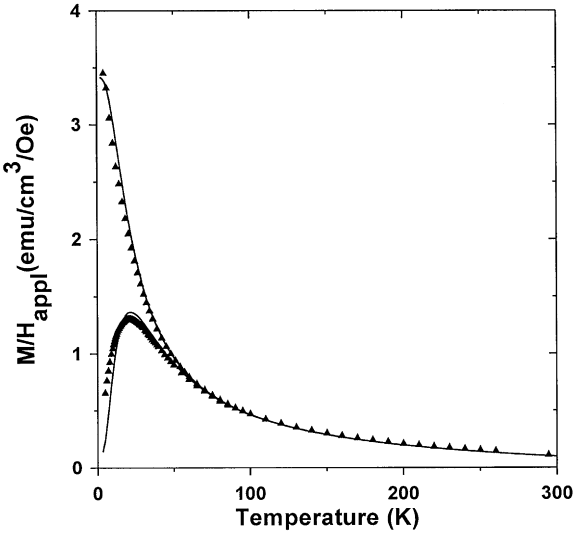

Fig. 13. The FC and ZFC initial susceptibilities for the sample 36A(C/50), measured (▲) and calculated (solid line); $H_{appl} = 5$ Oe acts parallel to the sample plane.

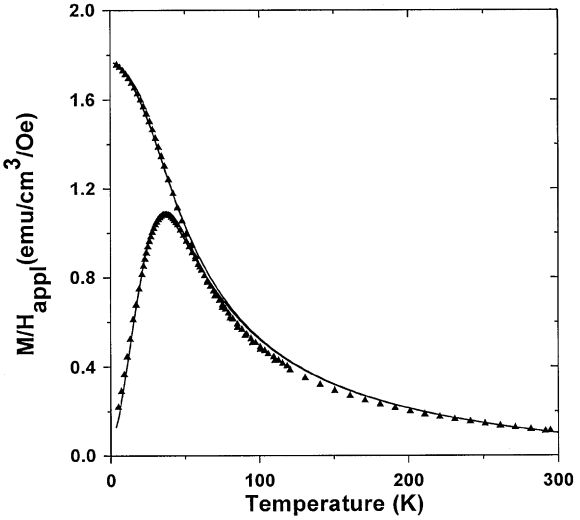

Fig. 14. The FC and ZFC initial susceptibilities for the sample 36A(C/1), measured (▲) and calculated (solid line); $H_{appl} = 5$ Oe acts parallel to the sample plane.

The instantaneous field acting at a particle site could be calculated using the Onsager model. The particle environment was replaced by a homogeneous and isotropic continuous medium, having a temperature-dependent initial permeability which was calculated in a self-consistent manner for both the FC and ZFC processes. The medium reaction to the particle dipole moment was shown to increase the particle anisotropy

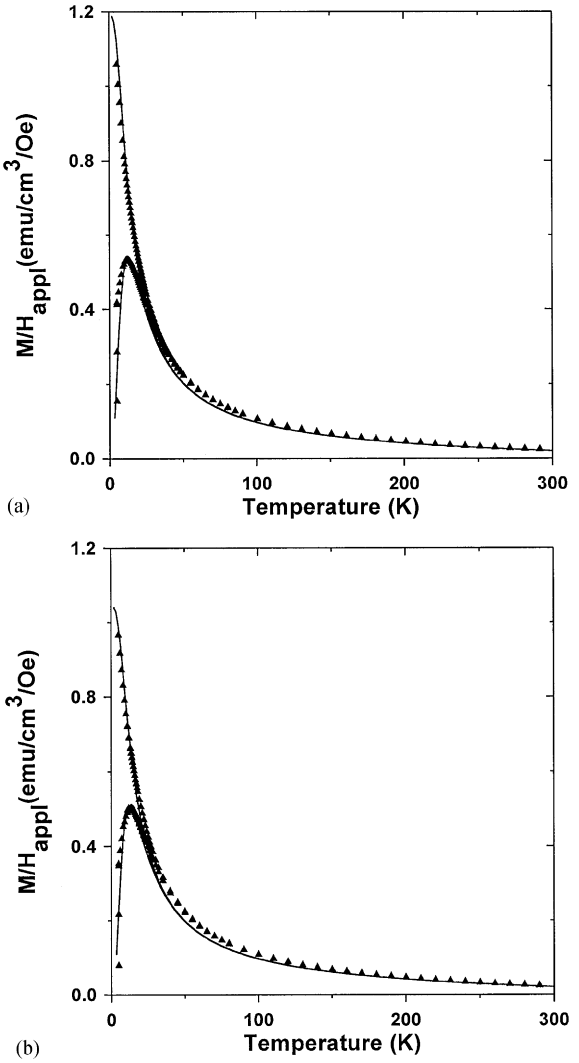

Fig. 15. The FC and ZFC initial susceptibilities for the sample 51A(C/50), measured (▲) and calculated (solid line); $H_{appl} = 15$ Oe acts parallel (a) respectively perpendicular (b) to the sample plane.

with increasing sample volume concentration. Due to the tensor character of the medium permeability in the particle neighborhood, this reaction could give rise to a uniaxial anisotropy under the circumstances of a uniaxial symmetry of the particle arrangement. The occurrence of a reaction anisotropy was interpreted using a distorted cavity, the particle agglomeration along a certain direction being studied through the variation of the Onsager cavity shape according to the space symmetry of the particle cluster. Thus, we suggest that the emergence of an interaction anisotropy is the consequence of the particle tendency of forming chains. This could also justify the hypothesis of Dormann [1] about the existence of a privileged axis for the particle moments fluctuations, which could be the chain axis. The Onsager model enables to distinguish between the contributions of the blocked and superparamagnetic particle fractions to the

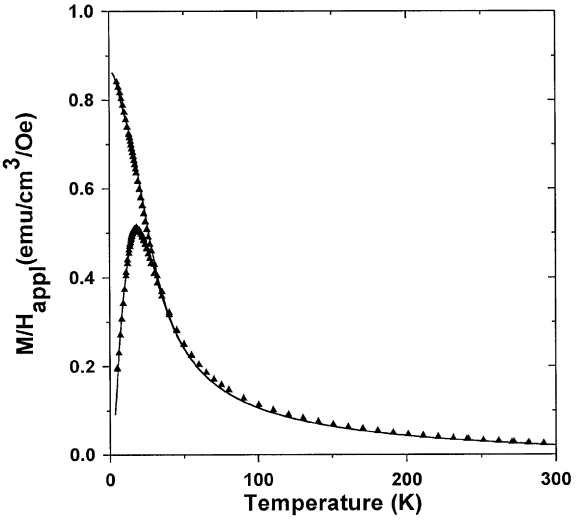

Fig. 16. The FC and ZFC initial susceptibilities for the sample 51A(C/1), measured (▲) and calculated (solid line); $H_{appl} = 15$ Oe acts parallel to the sample plane.

Table 3

Sample	H_{appl} (Oe)	Fit results										
		FC		ZFC		N		C				a/c
		A ($\times 10^3$ Oe)	T^* (K)	A ($\times 10^3$ Oe)	T^* (K)	P	N	P		N		
								FC	ZFC	FC	ZFC	
26A(C/50)	5	0	–	0	–	0	–	0.98	0.91	–	–	1
26A(C/1)	5	18.5	130	24	73	0	–	0.6	0.57	–	–	1.5
4D(C/50)	5	0	–	2.5	50	0.3	0.7	0.67	–	0.68	0.68	1
4D(C/25)	5	3.4	50	5.2	50	0	–	1	1	–	–	1
4D(C/5)	1	4.9	40	7	40	0	0.9	1	1	0.98	1.05	1.7
4D(C/1)	1	7.3	50	19	50	0	0.9	0.7	0.7	0.7	0.7	1.6
36A(C/50)	5	0	–	4	40	0	–	0.35	0.38	–	–	1
36A(C/1)	5	4.6	20	11	20	0.1	–	0.54	0.41	–	–	1.5
51A(C/50)	15	0	–	0	–	0	1	0.57	0.57	0.57	0.57	1
51A(C/1)	15	10	15	14	15	0	–	0.75	0.75	–	–	1.7

reaction anisotropy, which is not possible in the model of Dormann, given the assumption about the equilibrium of the thermal fluctuations.

We have assumed that the local non-homogeneity of the particle dispersion gives rise to an interaction field distribution, which was formally introduced via a representative field, temperature-dependent according to a given law whose parameters were identified by comparison with the experiment. One remarks that the

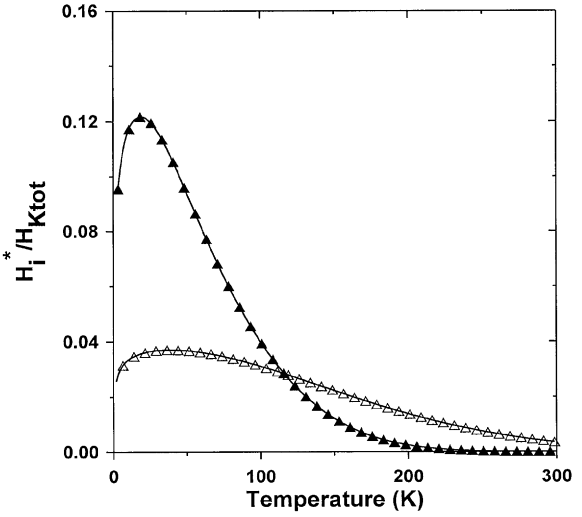

Fig. 17. The reduced interaction field $h_i^*(T) = H_i^*(T)/H_{K_{tot}}(T)(H_{K_{tot}} = 2K_{tot}(T)/M_S(T))$ in the FC (blank symbols) and ZFC (black symbols) processes, for the sample 26A(C/1) (▲).

effect of such a field is to diminish the medium initial susceptibility, especially in the low-temperature domain, due to the approach to saturation of the superparamagnetic particle fraction magnetization, which could give rise to a similar effect as an increasing anisotropy concerning the shift of the T_{MAX} temperature towards higher values, though the causes are totally different. An anisotropy, like the reaction anisotropy, increases the energy barriers, and thus, results in a slower increase of the critical volume with increasing temperature, giving rise to a shift of the T_{MAX} temperature towards higher values. On the contrary, a distribution of interaction fields shifts the critical temperature spectrum towards lower values. In this case, the critical volume increases faster with increasing temperature but, because the superparamagnetic susceptibility rapidly decreases with increasing field (the faster so as the temperature is lower), the superparamagnetic magnetization exhibits a saturation tendency which results in a lowering of the medium's (global) initial susceptibility. Also, the shift of the critical temperature spectrum towards lower values, due to the interaction field distribution (which creates field non-linear effects on the particle magnetization), enhances the latter effect by augmenting the contribution of the superparamagnetic fraction to the low-temperature medium (global) susceptibility. Thus, we conclude that the interaction anisotropy effect is not only a consequence of increasing reaction anisotropy with increasing sample volume concentration, as previously stated in Ref. [1], but also the result of the increasing magnitude of the distributed interaction fields.

The comparison between the theory and experiment shows that for the FC process, the interaction field H_i^* is systematically lower than that corresponding to the ZFC process. This could be noticed in Table 3 for the absolute values of the interaction field H_i^* and also for the reduced interaction fields h_i^* in Figs. 17–20. In our opinion, this is a consequence of the fact that at low temperatures, where the interaction field distribution is effective, there is a difference between the particle magnetic states in the two processes. In the FC process, the particle magnetic moments present a higher ordering degree than in the ZFC process. Thus, it is possible that, in the FC process, the volume density of the magnetic charges tends to be lower than in the ZFC process, leading to a narrowing of the interaction field distribution in the case of the FC process with respect to the ZFC process.

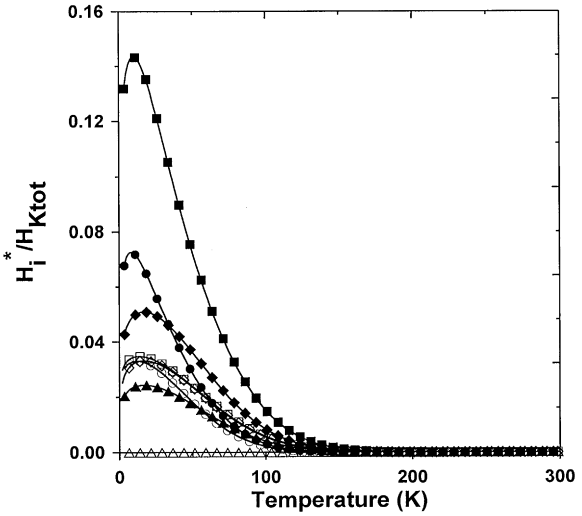

Fig. 18. The reduced interaction field $h_i^*(T)$ in the FC (white symbols) and ZFC (black symbols) processes, for the samples 4D(C/50) (▲), 4D(C/25) (◆), 4D(C/5) (●) and 4D(C/1) (■).

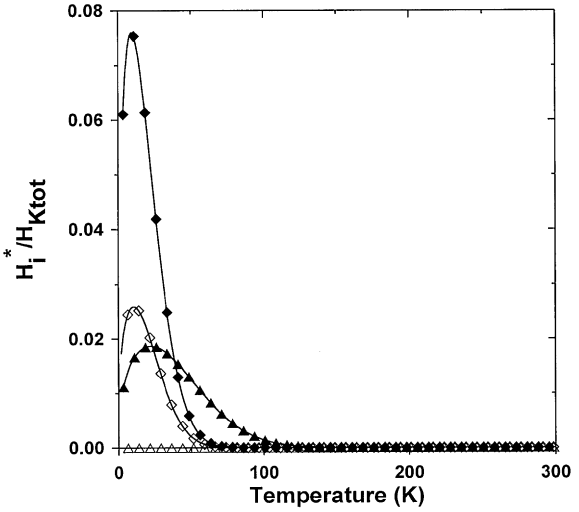

Fig. 19. The reduced interaction field $h_i^*(T)$ in the FC (white symbols) and ZFC (black symbols) processes, for the samples 36A(C/50) (▲) and 36A(C/1) (◆).

In Figs. 17–20 one notices that the non-linear interaction field H_i^* is effective in the temperature domain where the transition between the superparamagnetic and blocked states takes place. Furthermore, we have noticed that H_i^* is approximately proportional to the blocked particle fraction, suggesting that the interaction field distribution could be assigned to the blocked particles.

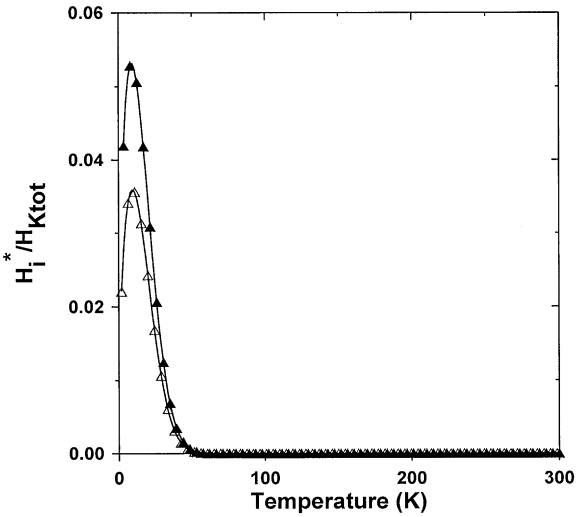

Fig. 20. The reduced interaction field $h_i^*(T)$ in the FC (white symbols) and ZFC (black symbols) processes, for the sample 51A(C/1) (▲).

Acknowledgements

The author would like to acknowledge the financial support offered by the French Government in the frame of a Réseau Formation Recherche Program during a one year stage at the University of Versailles LMOV. Also, Dr. M. Noguès is gratefully thanked for having taught the author to handle the SQUID magnetometer, and for providing additional experimental results.

References

[1] J.L. Dormann, L. Bessais, D. Fiorani, J. Phys. C 21 (1988) 2015.
[2] J.L. Dormann, F. D'Orazio, F. Lucari, E. Tronc, J.P. Jolivet, D. Fiorani, R. Cherkaoui, M. Nogues, Phys. Rev. B 53 (21) (1996) 14291.
[3] J.L. Dormann, D. Fiorani, E. Tronc, Adv. Chem. Phys. 98 (1997) 283.
[4] J.L. Dormann, in: J.L. Dormann, D. Fiorani (Eds.), Studies of Magnetic Properties of Fine Particles and their Relevance to Materials Science, Elsevier, Amsterdam, 1992, p. 115.
[5] M. El-Hilo, K. O'Grady, R.W. Chantrell, J. Magn. Magn. Mater. 117 (1992) 21.
[6] M. El-Hilo, K. O'Grady, R.W. Chantrell, J. Magn. Magn. Mater. 114 (1992) 295.
[7] M. El-Hilo, K. O'Grady, R.W. Chantrell, J. Magn. Magn. Mater. 114 (1992) 307.
[8] R.W. Chantrell, E.P. Wohlfarth, J. Magn. Magn. Mater. 40 (1983) 1.
[9] R.W. Chantrell, M. Fearon, E.P. Wohlfarth, Phys. Stat. Sol. (a) 97 (1986) 213.
[10] S. Shtrikman, E.P. Wohlfarth, J. Magn. Magn. Mater. 31–34 (1983) 1421.
[11] S. Shtrikman, E.P. Wohlfarth, Phys. Lett. A 85 (8, 9) (1981) 467.
[12] E.P. Wohlfarth, Phys. Lett. A 70 (5, 6) (1979) 489.
[13] R.W. Chantrell, M. El-Hilo, K. O'Grady, IEEE Trans. Magn. 27 (4) (1991) 3570.
[14] S. Morup, Europhys. Lett. 28 (9) (1994) 671.
[15] P. Prené, Thèse, Univ. P. et M. Curie, Paris, 1995.
[16] E. Tronc, J.P. Jolivet, in: J.L. Dormann, D. Fiorani (Eds.), Studies of Magnetic Properties of Fine Particles and their Relevance to Materials Science, Elsevier, Amsterdam, 1992, p. 199.

[17] L. Néel, J. Phys. Rad. 15 (4) (1954) 225.
[18] C. Papusoi Jr., J. Magn. Magn. Mater., accepted for publication.
[19] C. Papusoi Jr., Al. Stancu, J.L. Dormann, J. Magn. Magn. Mater. 174 (1997) 236.
[20] H. Pfeiffer, R.W. Chantrell, J. Magn. Magn. Mater. 120 (1993) 203.
[21] L. Onsager, J. Amer. Chem. Soc. 58 (1936) 1486.
[22] E.C. Stoner, E.P. Wohlfarth, Phil. Trans. Roy. Soc. A 240 (1948) 599.
[23] H. Pfeiffer, Phys. Stat. Sol. (a) 120 (1990) 233.
[24] H. Pfeiffer, Phys. Stat. Sol. (a) 122 (1990) 377.
[25] R.W. Chantrell, N.Y. Ayoub, J. Popplewell, J. Magn. Magn. Mater. 53 (1985) 199.